



Simultaneous and selective determination of purine metabolites in human urine samples using nanocomposite modified glassy carbon electrode

Xiaojian Liu^a, Jindong Dai^a, Jian Shen^a, Dongwei Zhu^a, Kanagaraj Raialakshmi^{a,*},
Selvaraj Muthusamy^{a,*}, Thangamani Kanagaraj^a, Palanisamy Kannan^{b,*}

^a Department of Gynecology, The Affiliated People's Hospital, and Department of Immunology, Jiangsu Key Laboratory of Laboratory Medicine, School of Medicine, and School of Chemistry and Chemical Engineering, Jiangsu University, Zhenjiang 212013, PR China

^b College of Biological, Chemical Sciences and Engineering, Jiaxing University, Jiaxing, Zhejiang 314001, PR China

ARTICLE INFO

Keywords:

Carbon nanotube
Polymer
Composite
Simultaneous determination
Lowest limit of detection

ABSTRACT

Herein, we reported the acid functionalized multiwalled carbon nanotubes (FMWCNTs) entrapped with polymer films derived from 3-amino-5-mercapto-1,2,4-triazole (AMTa) substrate sensitive and selective determination of purine metabolites in human urine samples. The FMWCNTs are covalently assembled on the GCE by simple carbodiimide coupling with diamine self-assemble monolayer (SAM) modified GCE. The nanocomposite on electrode surface is developed by electrochemical polymerization of AMTa over the FMWCNTs modified GCE (FMWCNTs/p-AMTa). The SEM images clearly shows the uniform deposition of p-AMTa on the surface walls of FMWCNTs, especially the diameter of the FMWCNTs is notably increased from 38 to 45 nm after the deposition of p-AMTa film on FMWCNTs. The nanocomposite was then exploited for the simultaneous and selective detection of purine metabolites. The alteration in the concentration of any one of purine metabolites can also change the concentration of next degradation metabolite, which leads to several critical diseases in our body. Thus, the simultaneous and sensitive determination of purine metabolites (uric acid, xanthine, hypoxanthine and inosine) using FMWCNTs/p-AMTa nanocomposite electrode is of high importance in clinical and healthcare aspects. In particular, the nanocomposite electrode shows higher electrocatalytic activity and a low limit of detection (LOD) toward these purine metabolites over the reported procedures. The practicability of the present approach is verified with urine samples and displays good recovery results.

1. Introduction

Uric acid (7,9-dihydro-1H-purine-2,6,8(3H)-trione, UA), Xanthine (3,7-dihydropurine-2,6-dione, XN), Hypoxanthine (1,7-dihydro-6H-purin-6-one, HXN) and Inosine (9-β-D-ribofuranosylhypoxanthine, INO) are of important purine degradation metabolites in human body (Scheme 1) [1]. In the presence of purine nucleotide phosphorylase enzyme INO converts into HXN. The transformation of HXN to XN and XN to UA takes place in the presence of xanthine oxidase [2]. Higher serum UA levels are mainly associated with risk of cardio-vascular disease, peripheral arterial illness, chronic kidney injury and silent brain-infarction [3]. Reduced level of plasma UA leads to Schizophrenia, sleep disordered breathing, multiple sclerosis, sex and age [4,5]. Normally, in serum UA exists in the range of 0.24 to 0.52 mM and from 1.4 to 4.4 mM in urine excretion [6,7]. XN is a well-known intermediate metabolite of purine nucleotide and naturally occurring purine

derivative in our body, and acts as an indicator of hypoxia [8]. HXN metabolized in human blood, induces the platelet aggregation and fastens the process of hemostasis or thrombosis [9]. The high concentration of HXN in blood leads to hypoxia in humans. This is mainly due to the inhibition of xanthine oxidase, which leads to expelling of molecular oxygen and superoxide radicals. These reactive oxygen species involve a foremost role in micro vascular issue and lead to direct tissue injury, lipid-peroxidation, denaturation of proteins and oxidation of DNA [10,11]. INO is a purine nucleoside and it is related with various sclerosis, shields against myocardial and anti-inflammatory effects [12]. A single dose of 20 mg of oral INO can elevated the urinary HXN and XN concentrations [13]. It is found in mRNA and mostly rich in brain mRNA [14]. It induces axonal rewiring and improves the behavior of outcome of stroke [15]. It inhibits the inflammatory effects of cytokine production [15]. In biological fluids, it is extremely very low concentration and rarely exceeds 100 nM [16].

* Corresponding authors.

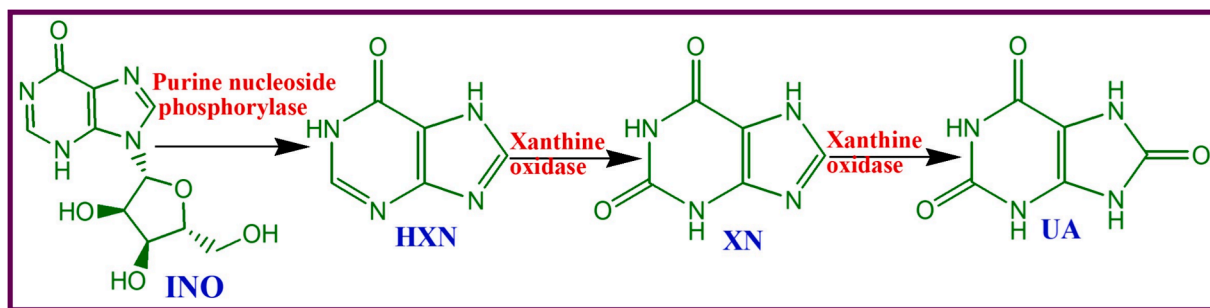
E-mail addresses: rajichen89@ujs.edu.cn (K. Rajalakshmi), rajselva311@ujs.edu.cn (S. Muthusamy), ktpkannan@zjxu.edu.cn (P. Kannan).

<https://doi.org/10.1016/j.molliq.2024.125845>

Received 24 July 2024; Received in revised form 16 August 2024; Accepted 22 August 2024

Available online 25 August 2024

0167-7322/© 2024 Elsevier B.V. All rights are reserved, including those for text and data mining, AI training, and similar technologies.



Scheme 1. Purine metabolic pathway.

UA, XN, HXN and INO are normally present in the body fluids at low concentrations [17,18]. The concentration levels of UA, XN, HXN and INO is a useful tool for monitoring the progression of diabetic without nephropathy patients [19,20]. The abnormal concentrations of any one of these metabolites lead to create some pathologic states along with xanthinuria, hyperuricemia, renal-failure, gout and toxemia during pregnancy [21,22]. The concentration level of these purine degradation metabolites in biological fluids such as human urine and blood serum are biomarkers for many clinically important diseases [23,24]. Hence, an precise quantification of UA, XA, HXN and INO in biological fluids are clinically vital to diagnose the related diseases in early stages. Several techniques were reported for the detection of purine degradation metabolites i.e., high-performance liquid chromatography (HPLC)[25] capillary electrophoresis [26] and electrochemical method [27–30]. In HPLC method, the detection wavelengths were of 260, 254, 254, 270 and 292 used toward the detection of purine metabolites adenosine, INO, HXN, XN and UA, respectively. The peaks for INO and HXN were overlapped each other. Hence, the determining the concentration of these purine metabolites separately is possible but the simultaneous determination of them is difficult by using HPLC method [31].

Recently, electrochemical biosensors are receiving huge attention due to their inexpensive, easy handling and time-consuming process [32–34]. Several reports were potentially described on the concurrent detection of these three purine metabolites UA, XN and HXN; UA, HXN and INO and XN, HXN and INO [35–40]. However, the simultaneous determination of UA, XN, HXN and INO yet to be reported; Keeping these objectives in mind, in the present study we made an attempt for concurrent detection of UA, XN, HXN and INO using FMWCNTs/p-AMTa nanocomposite modified GCE. The FMWCNTs/p-AMTa composite modified GCE showed 2.9-, 5.5-, 5.3- and 3.3-fold enhanced oxidation

current and 50, 80, 30 and 70 mV less positive potential oxidation towards the UA, XN, HXN and INO, respectively. In differential pulse voltammogram (DPV), it shows 370, 320 and 370 mV peak separation between UA-XN, XN-HXN and HXN-INO oxidation peaks, respectively. It is more than enough for simultaneous determination of these molecules. The sensitive determination of these purine degradation metabolites was achieved by amperometric technique in both linear and dynamic concentration ranges. The FMWCNTs/p-AMTa nanocomposite showed the significant lowest LOD toward these purine degradation metabolites and also used for practical detection of these compounds in human urine samples.

2. Experimental

2.1. Chemicals

AMTa, FMWCNTs, di-cyclohexylcarbodiimide (DCC), 1,8-octanedi-amine (OD), Uric acid (UA), Xanthine (XN), Hypoxanthine (HXN) and Inosine (INO) were received from Merck, India. For scanning electron microscopy (SEM) image analysis, we used glassy carbon (GC) plate instead of glassy carbon electrode (GCE), which was received from Alfa Aesar, India.

2.2. Characterizations

The SEM images were collected on a VEGA3 TESCAN instrument equipped with LaB8 filament, which operating at 30 kV with a resolution of 2.0 nm. Electrochemical experiments were conducted by using CHI634B (CH Instruments, Austin, TX, USA) equipped with GCE (3 mm), Pt wire, and NaCl saturated Ag/AgCl as a working, counter electrode

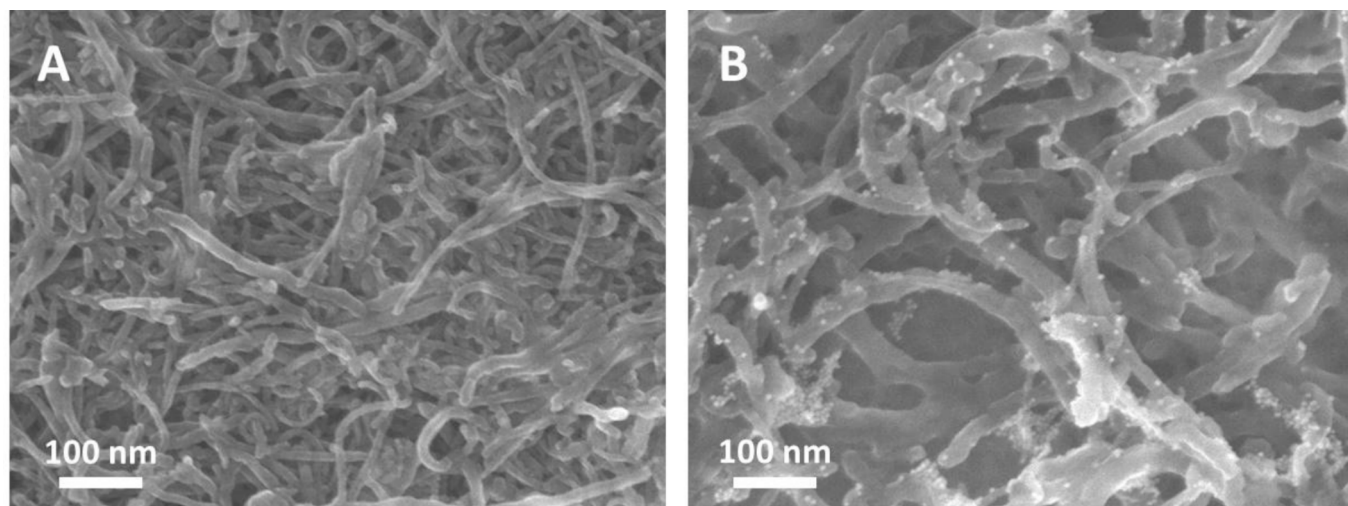


Fig. 1. SEM pictures obtained for GC/FMWCNTs (A) and GC/FMWCNTs/p-AMTa (B) substrates.

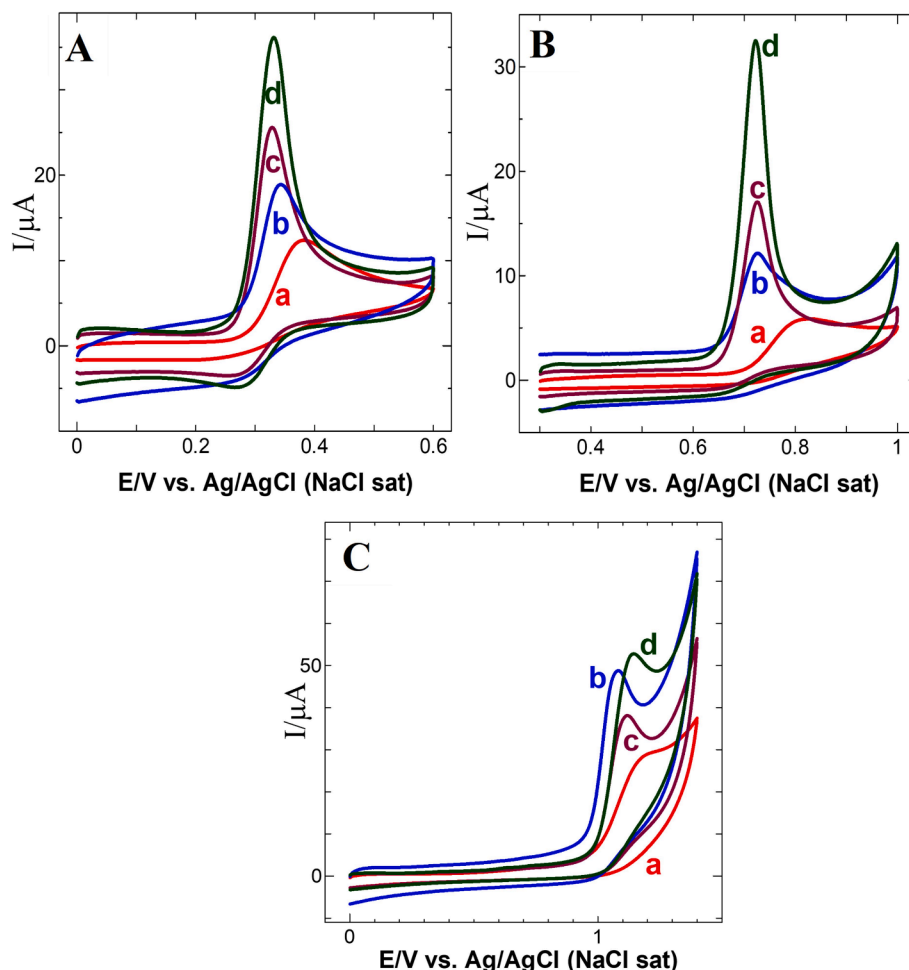


Fig. 2. CVs obtained for 0.5 mM of (A) UA, (B) XN and (C) HXN at (a) GCE, (b) GCE/FMWCNTs, (c) GCE/p-AMTa and (d) GCE/FMWCNTs/p-AMTa in PBS at a sweep rate of 50 mV/s.

and reference electrodes, respectively. For DPV analysis, an amplitude of 0.05 V, a pulse width of 0.06 s, a sample period of 0.02 s and a pulse time of 0.20 s were used.

2.3. Nanocomposite electrode fabrication

The treated GCE was soaked in 1 mM OD solution for 8 h, then the OD/GCE was rinsed with ethanol and ultrapure water for several times; subsequently, OD/GCE was then immersed in FMWCNTs (0.2 mg/ml) and DCC (2 mM) in an ethanolic solution (1:1) for 4 h. The condensation reaction takes place between acid group of FMWCNTs and the amine terminal of GCE/OD leading to the formation of amide bond, which enabled the assembly of FMWCNTs on the GCE/OD surface and it was denoted as GCE/FMWCNTs [41]. The FMWCNTs-polymer film electrode was obtained by electrochemical polymerization of 1 mM AMTa (15 cycles) between -0.2 and $+1.7$ V at a sweep rate of 50 mV s^{-1} in $0.1 \text{ M H}_2\text{SO}_4$ [42,43]. For comparison analysis, the bare GCE was polymerized with the identical condition to prepare the GCE/p-AMTa. The polymer modified GCEs were rinsed with water and stored in PBS solution for further use.

3. Results and discussion

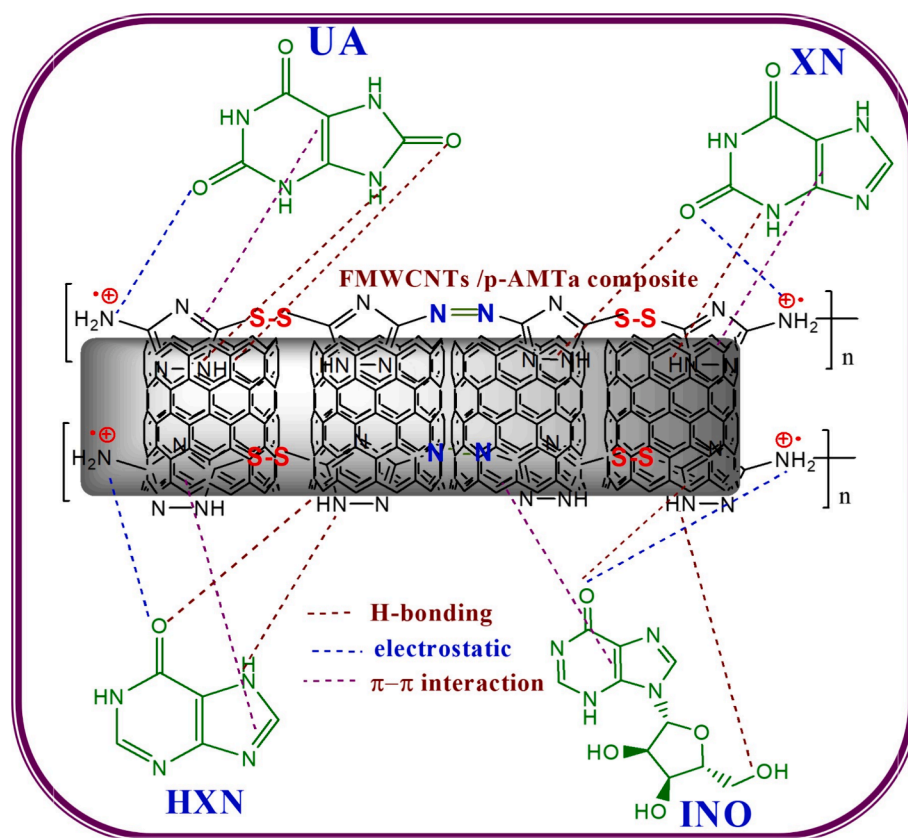
3.1. Surface characterization by SEM

The diameter and morphology of GC/FMWCNTs and GC/FMWCNTs/p-AMTa modified GCE substrates was examined by SEM

analysis. The networked larger bundles of tubular-like morphology of FMWCNTs were displayed in the Fig. 1A with a diameter of 38 nm and the length of $\sim 1\text{--}2 \mu\text{m}$. The presence of such larger CNTs bundles is owing to the attraction of FMWCNTs with bearing one through $\pi\text{--}\pi$ and van der Waals interactions [44]. Notably, Fig. 1B displayed the SEM picture of GC/FMWCNTs/p-AMTa substrate with some distorted arrangements of formed nanotubes. More importantly, the uneven distorted growth of p-AMTa polymeric films on the surface of FMWCNTs was explicitly observed. As a result, the average diameter of FMWCNTs was improved from 38 nm to 45 nm and these results were clearly revealed that, the effective formation of nanocomposites, i.e., the stable growth of p-AMTa films on the surface of FMWCNTs.

3.2. Electrochemical studies of FMWCNTs/p-AMTa nanocomposite

The CVs recorded for GCE/FMWCNTs/p-AMTa in a monomer-free $0.1 \text{ M H}_2\text{SO}_4$ solution at various scan rates from 25 to 175 mV/s and obtained result was shown in Figure S1. The CV result exhibited a notable oxidation peak at $+0.40 \text{ V}$ and respective reduction peak at $+0.34 \text{ V}$ with the peak separation of 60 mV. The above redox reaction was mainly attributed related to the addition and elimination (proton/electron) reactions at the --NH-- sites from the polymer film [45]. The surface coverage (Γ) of polymer nanocomposite film was obtained by $\Gamma = Q/nFA$. Where Q denoted as charge, n denoted as electrons involve in the redox reaction, F denoted as a Faraday constant (96485C), and A is surface area. The charge derived from anodic oxidation was applied to estimate the surface coverage without subtracting the surface roughness



Scheme 2. The possible interactions of UA, XN, HXN and INO with FMWCNTs/p-AMTa modified GCE.

factor. The surface coverage was determined as $9.58 \times 10^{-10} \text{ mol cm}^{-2}$ for p-AMTa on FMWCNTs. While applying different scan rates, the redox peak currents were enlarged linearly with a R^2 of 0.9980, indicating the redox reaction was due to surface bound species.

3.3. Electrochemical oxidation of UA, XN, HXN and INO

Fig. 2 displays the CVs profiles obtained for 0.5 mM UA, XN and HXN at GCE, GCE/p-AMTa, GCE/FMWCNTs and GCE/FMWCNTs/p-AMTa in 0.2 M PBS (pH 7.2). At bare GCE, oxidation of UA was occurred at 0.38 V (Fig. 2A: curve a). Notably, a slight drop in the current and less stability of peak potential (positive shift) were observed (Figure S2: curve a-dotted line) after five consecutive cycles. Next, the GCE/FMWCNTs exhibited a sharp anodic-oxidation peak for UA at 0.34 V, which is 1.2-times higher oxidation current response than GCE (Fig. 2A: curve b). Considerably, the oxidation peak response was continued unaffected (Figure S2A: curve b-dotted line). On the other side, the oxidation response peak was exhibited at 0.33 V (Fig. 2A: curve c) while using GCE/p-AMTa electrode, which is highly stable even after five continuous cycles (Figure S2A: curve c-dotted line). Interestingly, GCE/FMWCNTs/p-AMTa displayed a well-definite and stable oxidation response at 0.33 V with 2.9-fold improved anodic oxidation current and certainly the oxidation current response was about 50 mV less positive potential than the GCE for UA (Fig. 2A: curve d). To study the oxidation of XN, the GCE displayed an oxidation response toward XN at 0.80 V (Fig. 2B: curve a). The anodic peak current was varied towards more positive potential (0.85 V) with decreased peak current in the subsequent cycles (Figure S2B: curve a-dotted line). At GCE/FMWCNTs, the XN oxidized at 0.73 V (Fig. 2B: curve b) with an enhanced peak current when compare with bare GCE and also the peak was steady after five continuous cycles (Figure S2B: curve b-dotted line). A well-defined and stable oxidation response was identified for XN at 0.72 V with improved peak current at GCE/p-AMTa (Fig. 2B: curve c). The oxidation response

toward XN was about 5.5 and 3.9-fold higher at FMWCNTs/p-AMTa composite electrode when compared to GCE and GCE/FMWCNTs. The oxidation peak was appeared at 0.72 V (Fig. 2B: curve d) and it was quite stable (Figure S2B: dotted lines-curve d).

HXN shows an oxidation peak for Bare GCE at 1.17 V (Fig. 2C: curve a). Further cycles the oxidation peak current was decreased (Figure S2C: dotted line-curve a). The GCE/FMWCNTs shows a well-defined oxidation response for HXN at 1.08 V with a 5.5-fold higher anodic oxidation current than GCE (Fig. 2C: curve b) but the peak current was slightly decreased in the subsequent cycles (Figure S2C: dotted lines-curve b). While using GCE/p-AMTa, the HXN oxidation occurs at 1.12 V (Fig. 2C: curve c) and after five continuous cycles, the oxidation peak current was slightly decreased (Figure S2C: dotted lines-curve c). On the other side, GCE/FMWCNTs/p-AMTa showed a sharp anodic oxidation peak at 1.14 V with 5.3-fold improved current response toward HXN when correlated to GCE (Figure S2C: curve d) and the oxidation peak was extremely steady after five continuous cycles (Figure S2C: dotted lines-curve d).

LSV profiles recorded toward INO oxidation at GCE, GCE/p-AMTa, GCE/FMWCNTs and GCE/FMWCNTs/p-AMTa in 0.2 M PBS is shown in Figure S3. At bare GCE, INO showed an oxidation peak at 1.40 V (curve a) and it was slightly shifted after five continuous cycles (dotted line-curve a). The oxidation peak of INO was appeared at 1.34 V at GCE/FMWCNTs (curve b) and it was stable after five continuous cycles (dotted line-curve b). At GCE/p-AMTa, a well-defined and stable oxidation peak was obtained for INO at 1.34 V and the peak current was increased by 1.9-fold compared to bare GCE (curve c). The oxidation peak of INO was displayed at 1.34 V with 3.3-fold higher oxidation peak current at FMWCNTs/p-AMTa nanocomposite electrode than bare GCE (curve d). The oxidation response was highly stable after five continuous cycles (dotted line-curve d). In summary, unmodified GCE is not appropriate toward stable determination of these purine degradation metabolites owing to the experience of fouling-effect caused by adsorbed oxidation products on the surface of electrode. The FMWCNTs/p-

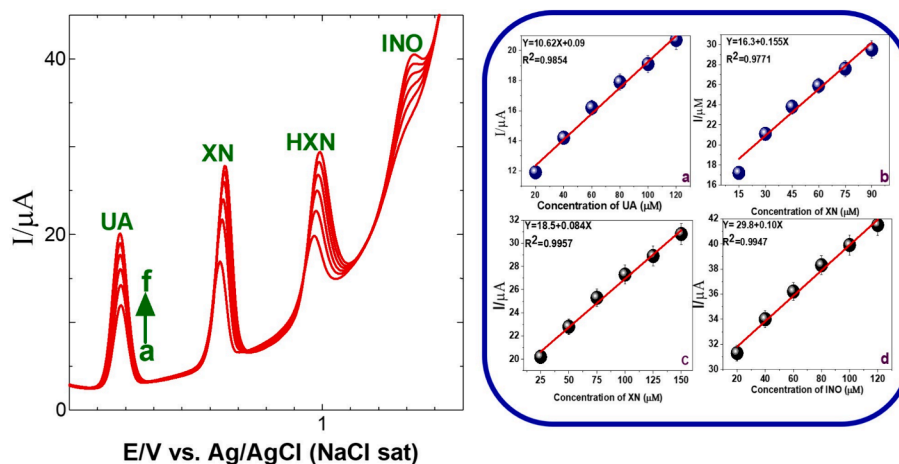


Fig. 3. DPVs of 20 μM UA, 15 μM XN, 25 μM HXN and 20 μM INO (curves a-f) at GCE/OD/FMWCNTs/p-AMTa in 0.2 M PBS. **Insets:** Plots of concentration of UA, XN, HXN and INO against the corresponding oxidation currents (a, b, c and d).

AMTa nanocomposite showed 50, 80, 30 and 70 mV less positive potential and 2.9, 5.5, 5.3 and 3.3-fold enhanced oxidation current toward the detection of UA, XN, HXN and INO, respectively.

3.4. Electro-oxidation mechanism

The displayed higher oxidation response (current) with low onset oxidation potential toward UA, XN, HXN and INO at p-AMTa film was mainly due to the presence of strong electrostatic and hydrogen bonding interaction between p-AMTa and the purine derivatives. On the other hand, π - π association between FMWCNTs and analyte molecules leads to higher current at OD/FMWCNTs modified electrode. The enhanced peak

current for the four analytes at the FMWCNTs/p-AMTa nanocomposite was ascribed to the presence of electrostatic and hydrogen bonding interaction between p-AMTa and the analyte molecules and π - π attraction between FMWCNTs and analytes molecules as shown in Scheme 2 [43,44].

3.5. Effect of scan rates

Figure S4 and S5 displayed the CVs, and LSVs profile toward 0.5 mM UA, XN, HXN and INO at GCE/FMWCNTs/p-AMTa at different scan rates. Notably, the oxidation current response was improved linearly with respect to scan rates. A good linear plot was obtained by plotting

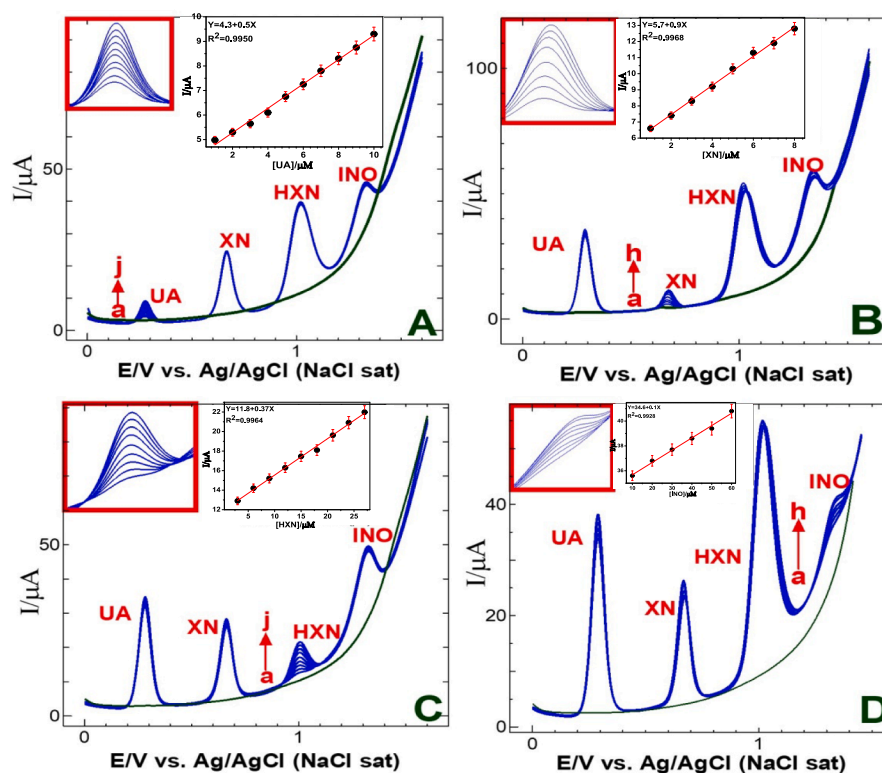


Fig. 4. DPVs obtained for (A) the addition (curves b-j) of 1 μM UA into 0.3 mM of XN, HXN and INO; (B) addition of 1 μM XN into 0.3 mM of UA, HXN and INO (curves b-h); (C) addition of 3 μM HXN into 0.3 mM of each UA, XN and INO (curves b-j) and (D) addition of 10 μM INO into 0.3 mM of UA, XN and HXN (curves b-h) at GCE/FMWCNTs/p-AMTa in 0.2 M PBS. **Insets:** Expanded views and their corresponding calibration plots.

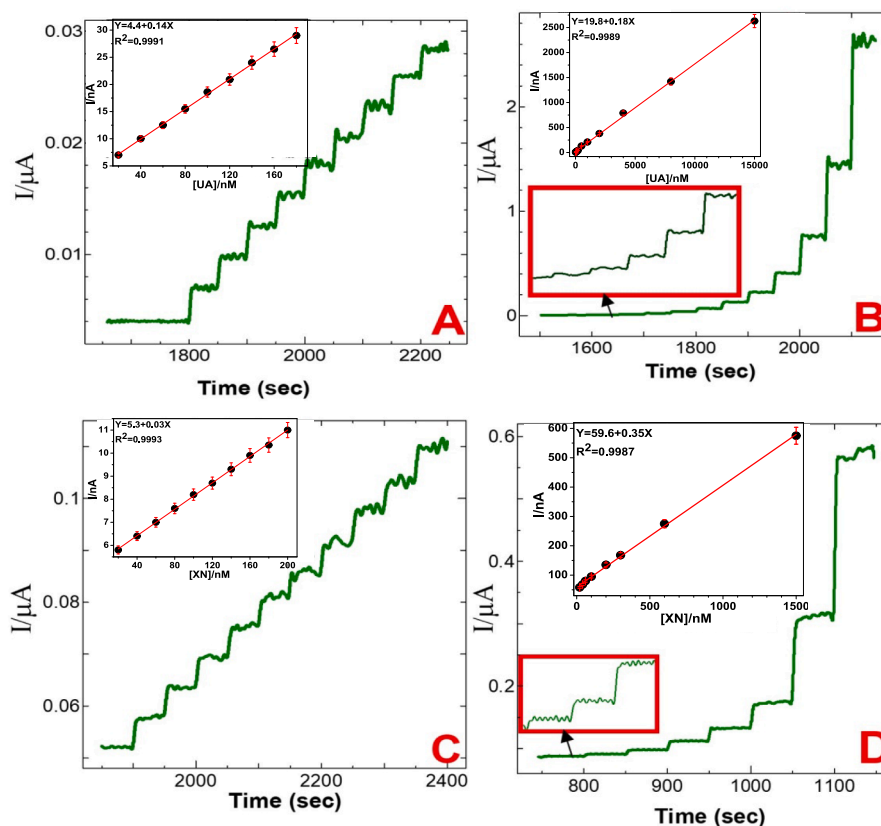


Fig. 5. Amperometric *i-t* profiles of UA and XN at GCE/FMWCNTs/p-AMTa in 0.2 M PBS. (A) 20 nM individual addition of UA and (B) concentrations of UA added from 10 nM to 40 μ M at an interval of 50 s. $E_{app} = +0.4$ V. (C) 20 nM individual addition of XN and (D) concentrations of XN added from 10 nM to 1500 nM at an interval of 50 s. $E_{app} = +0.8$ V. **Insets:** Respective calibration plots and expanded view.

anodic oxidation current response vs. square root of scan rates with the R^2 of 0.9983, 0.9937, 0.9989 and 0.9977 for UA, XN, HXN and INO, respectively (Insets of Figure S4 and S5), demonstrating the potential oxidation of these purine degradation metabolites were diffusion-controlled reaction.

3.6. Simultaneous analysis of UA, XN, HXN and INO at nanocomposite

To detect simultaneously about UA, XN, HXN and INO, the DPVs obtained for different concentrations of UA, XN, HXN and INO at GCE/FMWCNTs/p-AMTa electrode were shown in Fig. 3. A well separated oxidation responses were obtained for UA (20 μ M), XN (15 μ M), HXN (25 μ M), and INO (20 μ M) at 0.28, 0.65, 0.97 and 1.37 V, respectively (curve a). The oxidation peak separation between the UA-XN, XN-HXN and HXN-INO were of 370, 320 and 370 mV, respectively. It is more than enough to determine these purine degradation metabolites simultaneously. When the concentration of UA and INO were used from 20 μ M to 120 μ M; XN was used from 15 μ M to 90 μ M and HXN was used from 25 μ M to 150 μ M for the respective analytes, which were increased linearly (curves a-f). The plots of concentration of analytes with the oxidation currents show linearity with the correlation coefficients of 0.9970, 0.9930, 0.9865 and 0.9998 for UA, XN, HXN and INO, respectively (Insets: a, b, c and d, respectively).

3.7. Selective detection of UA, XN, HXN and INO at nanocomposite

The GCE/FMWCNTs/p-AMTa nanocomposite was exploited toward the selective detection of one of the purine metabolites in presence of higher concentrations of others. Fig. 4A displayed the selective detection of UA in presence of higher concentrations of XN, HXN and INO. The oxidation peak for 1 μ M of UA was obtained at 0.28 V for the solution

containing 0.3 mM of XN, HXN and INO. Each addition of 1 μ M of UA up to 10 μ M to mixed solution, the peak current at 0.28 V was improved linearly (Inset: Fig. 4A) with the R^2 of 0.9923, and the oxidation peaks potential and current for XN, HXN and INO were stable and constant. Fig. 4B displayed the selective detection of XN in presence of higher concentrations of other three metabolites. For 1 μ M of XN, the oxidation response was obtained at 0.67 V in presence of 0.3 mM of UA, HXN and INO. Individual addition of 1 μ M of XN to the above mixed solution, the oxidation peak current increases dynamically with the R^2 0.9976 (Inset: Fig. 4B). The oxidation peaks current and potentials obtained for UA, HXN and INO were remaining unchanged. DPVs obtained for 3 μ M of HXN in 0.3 mM of UA, XN and INO are shown in Fig. 4C. A well-defined peak was observed for HXN at 1.0 V even in presence of 100-fold excess of UA, XN and INO. The oxidation response was directly proportional to the concentrations range of 3–21 μ M of HXN. The plot of concentration versus the oxidation current is shown in Inset: Fig. 4C. The correlation coefficient was found to be 0.9980. Similarly, 10 μ M of INO in presence of 0.3 mM of UA, XN and INO showed an oxidation response at 1.30 V for INO (Fig. 4D). Further, the concentration of INO was used from 20 to 70 μ M (c-h), the oxidation current response was improved linearly without shifting the oxidation potential of other analytes. The expanded view of INO current increment and the linear plot of (INO concentration vs. oxidation current) were shown in Inset: Fig. 4D.

3.8. Amperometric detection of UA, XN, HXN and INO

The sensitivity of FMWCNTs/p-AMTa nanocomposite was studied towards the detection of UA, XN, HXN and INO was examined by amperometric method. Fig. 5A–D, Fig. 6A–D showed the *i-t* curve responses toward the oxidation of UA, XN (Fig. 5A–D), HXN and INO (Fig. 6A–D) in a constantly stirred 0.2 M PBS by using constant applied

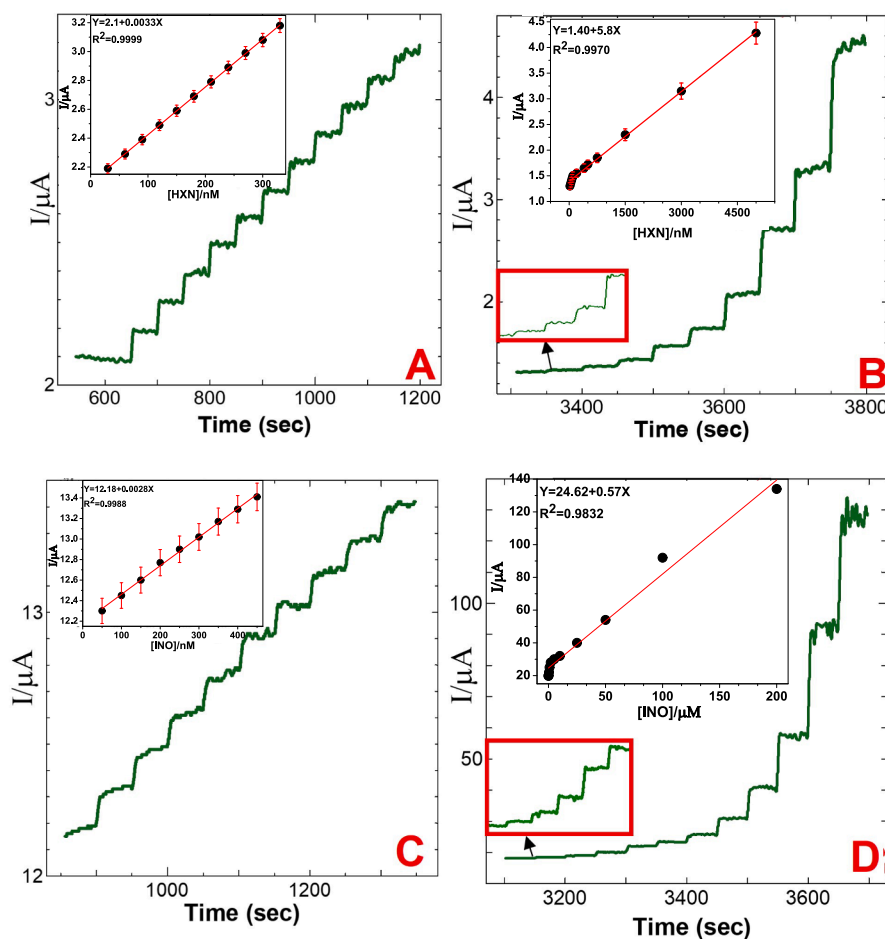


Fig. 6. Amperometric *i-t* curve of HXN and INO at GCE/FMWCNTs/p-AMTa in 0.2 M PBS. (A) 30 nM individual addition of HXN and (B) the concentrations of HXN added from 20 nM to 5000 nM at an interval of 50 s. $E_{app} = +1.1$ V. (C) 50 nM individual addition of INO by and (D) the concentrations of XN added from 10 nM to 40 μ M at an interval of 50 s. $E_{app} = +1.35$ V. **Inset(s):** Respective calibration plots and expanded view.

potential of 0.4, 0.8, 1.1 and 1.35 V toward UA, XN, HXN and INO, respectively. The GCE/FMWCNTs/p-AMTa showed the original response during the addition of 20 nM of UA (Fig. 5A). Further addition of 20 nM UA in further steps with a interval of 50 s, the current response was linearly increased with a R^2 of 0.9994 (Inset: Fig. 5A). The amperometric current response was also increased linearly with the dynamic range of 10 nM–40 μ M of UA (Fig. 5B) with a R^2 of 0.9997 (Inset: Fig. 5B) and the LOD was found to be 0.5 nM ($S/N=3$). The GCE/FMWCNTs/p-AMTa showed the initial current response toward the addition of 20 nM XN (Fig. 5C). Further increase the concentration of XN in every addition with the interval of 50 s. The linear dependence toward oxidation current response of XN was steady from 10 to 1500 nM (Fig. 5C) with a R^2 of 0.9987 (Inset: Fig. 5D) and the LOD was found to be 0.4 nM ($S/N=3$). The GCE/FMWCNTs/p-AMTa showed the initial current response toward the addition of 30 nM HXN (Fig. 6A). The *i-t* current response was increased steadily during addition of 30 nM HXN in every step with the interval of 50 s and the R^2 of 0.9999 (Inset: Fig. 6B). The *i-t* current profile was also raised linearly while adding HXN from 20 nM to 5000 nM HXN (Fig. 6C) with the R^2 of 0.9974 (Inset: Fig. 6D) and the LOD was about 0.6 nM ($S/N=3$). The GCE/FMWCNTs/p-AMTa showed the current response toward the addition of 50 nM INO (Fig. 5G). The linear dependence response of INO from 10 nM to 40 μ M with the R^2 of 0.9844 (Inset: Fig. 5H) and the LOD was about 0.3 nM ($S/N=3$). Further, the sensitivity of the composite electrode towards UA, XN, HXN and INO was found to be 0.14, 0.03, 3.3 and 2.8 nA/nM, respectively. The LOD obtained toward UA, XN, HXN and INO in this study was compared with recent reports (Table S1).

As shown in Table S1, the present GCE/FMWCNTs/p-AMTa electrode showed the lowest LOD toward UA, XN, HXN and INO when compared to the other nanocomposites [38–48]. Further, the fabrication of GCE/FMWCNTs/p-AMTa electrode is simple and efficient. For example, the acetylene-black/dihexadecyl hydrogen phosphate was prepared by mixing an equal amount of acetylene-black and dihexadecyl hydrogen phosphate in water and it was sonicated for 5 h. The resulted black product was casted on the surface of GCE and then the electrode was treated by CV cycling between 0.0 and 1.0 V in 0.1 M PBS (pH 8.0) for further use [43].

3.9. Determination of UA, XN, HXN and INO in urine sample

The practical utility of FMWCNTs/p-AMTa nanocomposite was evaluated by screening the concentrations of UA, XN, HXN and INO in human urine samples. The standard addition method was used for the detection of all analyte molecules. The DPV profiles obtained for 10 times diluted urine samples in PBS Fig. 7; curve a) and after added the commercial UA, XN, HXN and INO into the same mixture. The urine sample displayed an oxidation peak at 0.28, 0.65, 0.97 and 1.34 V, which were corresponded to UA, XN, HXN and INO, respectively (Fig. 7; curve b).

To check the peaks at 0.28, 0.65, 0.97 and 1.34 V of the urine sample are due to UA, XN, HXN and INO commercially available UA, XN, HXN and INO were added to the same solution. The peak currents were increased at the same potential after the addition of them. Based on the obtained oxidation currents, their concentrations in different samples

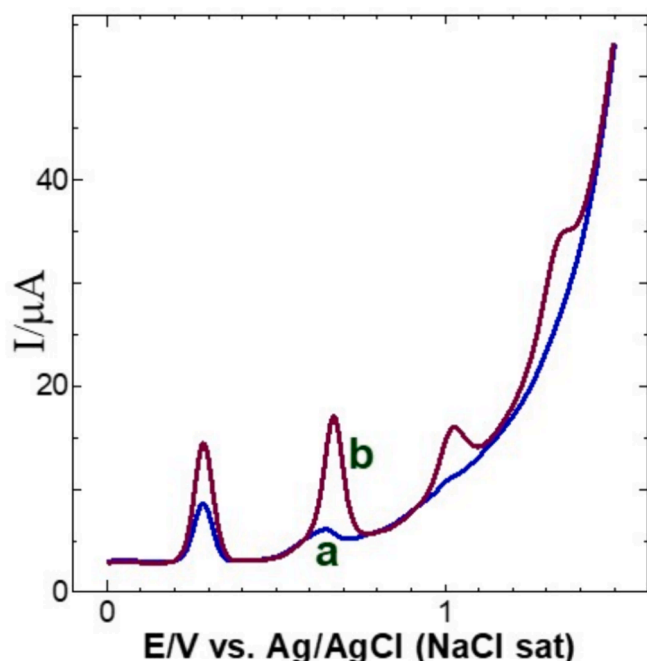


Fig. 7. DPVs of (a) diluted urine sample and (b) after the addition of UA, XN, HXN and INO in 0.2 M PBS at GCE/OD/FMWCNTs/p-AMTa.

were calculated. The actual and estimated concentrations and their recoveries were represented in Table S2. This indicates that the GCE/FMWCNTs/p-AMTa can be efficiently used toward the simultaneously detection of UA, XN, HXN and INO in real samples. Further, the effect of pH at the surface of composite modified electrode was analyzed in 0.2 M PBS at different pH solutions. By increasing the pH from 3 to 10 both the oxidation and reduction peak potentials were shifted towards less positive potentials with good linearity (Fig. S6). The obtained results indicate that equal number of electrons and protons involved in the redox reaction at the composite modified electrode surface.

3.10. Stability and reproducibility

To study the stability, the GCE/FMWCNTs/p-AMTa was examined toward 0.5 mM of UA, XN, HXN and INO in 0.2 M PBS at every 300 s interval, and found that the peak currents remained same with a RSD of 1.1, 1.0, 0.9 and 1.2 % for UA, XN, HXN and INO, respectively, for 15 continuous analysis demonstrating the good reproducibility. Notably, the current response was slightly reduced to 1.2, 1.2, 1.4 and 1.5 % after 2 weeks toward UA, XN, HXN and INO, respectively. To determine the reproducibility, three-different GCE/FMWCNTs/p-AMTa was fabricated and their electrochemical response was studied toward the oxidation of 0.5 mM UA, XN, HXN and INO repeated measurements (15-times). The peak current RSD of 2.1, 2, 2.3 and 2 % were corresponded to UA, XN, HXN and INO, respectively, which obviously evidencing superior reproductivity.

4. Conclusions

We demonstrated the simple fabrication of FMWCNTs/p-AMTa nanocomposite film; the SEM images were clearly indicated the nanostructured conducting polymer uniformly deposited on the FMWCNTs surface. After the deposition of the p-AMTa, an average size of the FMWCNTs increased from 38 to 45 nm. Further, the nanocomposite electrode was utilized for the concurrent and selective detection of UA, XN, HXN and INO. The nanocomposite electrode showed 2.9, 5.5, 5.3 and 3.3-fold enhanced oxidation currents and 50, 80, 30 and 70 mV less positive potential oxidation than GCE toward the oxidation of UA, XN,

HXN and INO, respectively. The enhanced electrocatalytic behaviour at nanocomposite electrode was due to the combined effect of electrostatic, hydrogen bonding and π - π attractions. Notably, the composite modified GCE showed 370, 320 and 370 mV peak to peak separations between UA-XN, XN-HXN and HXN-INO, respectively. The nanocomposite showed a good sensitivity and linearity as well as dynamic range toward UA, XN, HXN and INO. The LOD of UA, XN, HXN and INO were found to be 0.5, 0.4, 0.6 and 0.8 nM, respectively. The practicality was confirmed by detecting these analytes in human urine samples with good recoveries.

CRedit authorship contribution statement

Xiaojian Liu: Visualization, Investigation, Data curation, Conceptualization. **Jindong Dai:** Formal analysis, Data curation. **Jian Shen:** Investigation, Formal analysis. **Dongwei Zhu:** Validation, Project administration, Funding acquisition. **Kanagaraj Rajalakshmi:** Writing – original draft, Supervision, Methodology, Conceptualization. **Selvaraj Muthusamy:** Writing – original draft, Methodology, Funding acquisition. **Thangamani Kanagaraj:** Data curation, Formal analysis. **Palanisamy Kannan:** Writing – review & editing, Supervision, Methodology.

Declaration of competing interest

The authors declare that they have no known competing financial interests or personal relationships that could have appeared to influence the work reported in this paper.

Data availability

No data was used for the research described in the article.

Acknowledgements

D.Z thanks to National Natural Science Foundation of China (Grant Nos. 82202001), X. L thanks for the Project of Jiangsu Provincial Administration of Traditional Chinese Medicine (MS2023144) and Project of Zhenjiang Science and Technology Bureau (SH2023066) and S. M Thanks to the National Natural Science Foundation of China (No. 22150410327).

Appendix A. Supplementary material

Supplementary material to this article can be found online at <https://doi.org/10.1016/j.molliq.2024.125845>.

References

- [1] Z. Huang, N. Xie, P. Illes, F. Di Virgilio, H. Ulrich, A. Semyanov, A. Verkhatsky, B. Sperlagh, S.-G. Yu, C. Huang, Y. Tang, From purines to purinergic signalling: molecular functions and human diseases, *Signal Transduct. Target. Ther.* 6 (2021) 162.
- [2] C. Hou, G. Xiao, W.K. Amakye, J. Sun, Z. Xu, J. Ren, Guidelines for purine extraction and determination in foods, *Food Front.* 2 (2021) 557–573.
- [3] Y. Si, H.J. Lee, Carbon nanomaterials and metallic nanoparticles-incorporated electrochemical sensors for small metabolites: Detection methodologies and applications, *Curr. Opin. Electrochem.* 22 (2020) 234–243.
- [4] W. Niu, H. Yang, C. Lu, The relationship between serum uric acid and cognitive function in patients with chronic heart failure, *BMC Cardiovasc. Disord.* 20 (2020) 381.
- [5] E. Humer, C. Pieh, G. Brandmayr, Metabolomics in sleep, insomnia and sleep apnea, *Inter. J. Mol. Sci.* 21 (2020) 7244.
- [6] S. Tvorynska, J. Barek, B. Josypczuk, Flow amperometric uric acid biosensors based on different enzymatic mini-reactors: A comparative study of uricase immobilization, *Sens. Actuat. B: Chem.* 344 (2021) 130252.
- [7] A. Saadati, F. Farshchi, M. Hasanzadeh, F. Seidi, A microfluidic paper-based colorimetric device for the visual detection of uric acid in human urine samples, *Anal. Meth.* 13 (2021) 3909–3921.

- [8] M. Furuhashi, New insights into purine metabolism in metabolic diseases: role of xanthine oxidoreductase activity, *Am. J. Physiol.-Endocrinol. Metabol.* 319 (2020) E827–E834.
- [9] P. Toledo-Ibelle, R. Gutiérrez-Vidal, S. Calixto-Tlacomulco, B. Delgado-Coello, J. Mas-Oliva, Hepatic accumulation of hypoxanthine: A link between hyperuricemia and nonalcoholic fatty liver disease, *Archiv. Med. Res.* 52 (2021) 692–702.
- [10] Y.G.C. Varadaiah, S. Sivanesan, S.B. Nayak, K.R. Thirumalarao, Purine metabolites can indicate diabetes progression, *Archiv. Physiol. Biochem.* 128 (2022) 87–91.
- [11] B. Singla, R.V. Aithabathula, S. Kiran, S. Kamil, S. Kumar, U.P. Singh, Reactive oxygen species in regulating lymphangiogenesis and lymphatic function, *Cells* 11 (2022) 1750.
- [12] C. Doyle, V. Cristofaro, M.P. Sullivan, R.M. Adam, Inosine – a multifunctional treatment for complications of neurologic injury, *Cell. Phys. Biochem.* 49 (2018) 2293–2303.
- [13] Y. Zhang, S. Guo, C. Xie, J. Fang, Uridine metabolism and its role in glucose, lipid, and amino acid homeostasis, *BioMed Res. Inter.* 2020 (2020) 7091718.
- [14] N. Dutta, I. Deb, J. Sarzynska, A. Lahiri, Inosine and its methyl derivatives: Occurrence, biogenesis, and function in RNA, *Prog. Biophys. Mol. Biol.* 169–170 (2022) 21–52.
- [15] S. Srinivasan, A.G. Torres, L. Ribas de Pouplana, Inosine in biology and disease, *Genes* 12 (2021) 600.
- [16] Y. Lu, L. Lin, J. Ye, Human metabolite detection by surface-enhanced Raman spectroscopy, *Mater. Today Bio.* 13 (2022) 100205.
- [17] L. Durai, S. Badhulika, Facile synthesis of large area pebble-like β -NaFeO₂ perovskite for simultaneous sensing of dopamine, uric acid, xanthine and hypoxanthine in human blood, *Mater. Sci. Eng. C* 109 (2020) 110631.
- [18] M.W. Ahmad, B. Dey, G. Sarkhel, D.-J. Yang, A. Choudhury, Sea-urchin-like cobalt-MOF on electrospun carbon nanofiber mat as a self-supporting electrode for sensing of xanthine and uric acid, *J. Electroanal. Chem.* 920 (2022) 116646.
- [19] C.-J. Chen, W.-L. Liao, C.-T. Chang, Y.-N. Lin, F.-J. Tsai, Identification of urinary metabolite biomarkers of type 2 diabetes nephropathy using an untargeted metabolomic approach, *J. Proteome Res.* 17 (2018) 3997–4007.
- [20] M. Luo, Z. Zhang, Y. Lu, W. Feng, H. Wu, L. Fan, B. Guan, Y. Dai, D. Tang, X. Dong, C. Yun, B. Hoher, H. Liu, Q. Li, L. Yin, Urine metabolomics reveals biomarkers and the underlying pathogenesis of diabetic kidney disease, *Inter. Urol. Nephrol.* (2022).
- [21] L.V. Dissanayake, A. Zietara, V. Levchenko, D.R. Spires, M. Burgos Angulo, A. El-Meanawy, A.M. Geurts, M.R. Dwinell, O. Palygin, A. Staruschenko, Lack of xanthine dehydrogenase leads to a remarkable renal decline in a novel hypouricemic rat model, *iScience* 25 (2022) 104887.
- [22] A.K. Yadav, D. Verma, R.K. Sajwan, M. Poddar, S.K. Yadav, A.K. Verma, P. R. Solanki, Nanomaterial-based electrochemical nanodiagnosics for human and gut metabolites diagnostics: Recent advances and challenges, *Biosensors* (2022).
- [23] A. Gallo, L.-E. Pillet, R. Verpillot, New frontiers in Alzheimer's disease diagnostic: Monoamines and their derivatives in biological fluids, *Exp. Gerontol.* 152 (2021) 111452.
- [24] P. Kubán, M. Dvořák, P. Kubán, Capillary electrophoresis of small ions and molecules in less conventional human body fluid samples: A review, *Anal. Chim. Acta* 1075 (2019) 1–26.
- [25] L. Kang, J. Liu, H. Zhang, M. Jiang, Y. Jin, M. Zhang, P. Hu, Improved ultra-high performance liquid chromatographic method for simultaneous determination of five gout-related metabolites in human serum, *J. Sep. Sci.* 44 (2021) 954–962.
- [26] M. Shah, N. Patel, N. Tripathi, V.K. Vyas, Capillary electrophoresis methods for impurity profiling of drugs: A review of the past decade, *J. Pharmaceut. Anal.* 12 (2022) 15–28.
- [27] Z. Panahi, L. Custer, J.M. Halpern, Recent advances in non-enzymatic electrochemical detection of hydrophobic metabolites in biofluids, *Sens. Actuat. Rep.* 3 (2021) 100051.
- [28] W. Wang, J. Cui, Y. Zhao, C. Ye, S. Zhou, X. Guo, C. Zhang, J. Li, D. Wu, A label-free approach to detect cell viability/cytotoxicity based on intracellular xanthine/guanine by electrochemical method, *J. Pharmacol. Toxicol. Meth.* 100 (2019) 106625.
- [29] S. Zhou, X. Guo, L. Meng, J. Cui, J. Li, X. Yuan, D. Wu, A miniature electrochemical detection system based on GOQDs/MWCNTs/SPCE* for determination the purine in cells, *Anal. Biochem.* 577 (2019) 67–72.
- [30] D. Zhu, X. Bai, P. Zhang, X. Li, An electrochemical sensor based on boron/nitrogen co-doped honeycomb-like porous carbon encapsulation molybdenum trioxides for the simultaneous detection of xanthine, uric acid and dopamine, *Colloids Surf. A* 655 (2022) 130304.
- [31] D.A. Mei, G.J. Gross, K. Nithipatikom, Simultaneous determination of adenosine, inosine, hypoxanthine, xanthine, and uric acid in microdialysis samples using microbore column high-performance liquid chromatography with a diode array detector, *Anal. Biochem.* 238 (1996) 34–39.
- [32] M. Baghayeri, A. Amiri, M. Fayazi, M. Nodehi, A. Wsmaeelnia, Electrochemical detection of bisphenol a on a MWCNTs/CuFe₂O₄ nanocomposite modified glassy carbon electrode, *Mater. Chem. Phys.* 261 (2021) 124247–124254.
- [33] M.G. Motlagh, M.A. Taher, M. Fayazi, M. Baghayeri, A. Hosseiniifar, Non enzymatic amperometric sensing of hydrogen peroxide based on vanadium pentoxide nanosturctures, *J. Electroanal. Chem.* 166 (2019) 367–372.
- [34] M. Baghayeri, H. Alinezhad, M. Tarahomi, M. Fayazi, M.G. Motlagh, B. Maleki, A non enzymatic hydrogen peroxide sensor based on dendrimer functionalized magnetic graphene oxide decorated with palladium nanoparticles, *Appl. Sur. Sci.* 478 (2019) 87–93.
- [35] M. Dervisevic, E. Dervisevic, M. Šenel, Recent progress in nanomaterial-based electrochemical and optical sensors for hypoxanthine and xanthine. A review, *Microchim. Acta* 186 (2019) 749.
- [36] O. Sarakhman, A. Benková, L. Švorc, A modern and powerful electrochemical sensing platform for purines determination: Voltammetric determination of uric acid and caffeine in biological samples on miniaturized thick-film boron-doped diamond electrode, *Microchem. J.* 175 (2022) 107132.
- [37] R.G. Krishnan, R. Rejithamol, B. Saraswathyamma, Non-enzymatic electrochemical sensor for the simultaneous determination of adenosine, adenine and uric acid in whole blood and urine, *Microchem. J.* 155 (2020) 104745.
- [38] M. Ganesan, K.D. Ramadhas, H.-C. Chuang, G. Gopalakrishnan, Synthesis of nitrogen-doped carbon quantum dots@Fe₂O₃/multiwall carbon nanotubes ternary nanocomposite for the simultaneous electrochemical detection of 5-fluorouracil, uric acid, and xanthine, *J. Mol. Liq.* 331 (2021) 115768.
- [39] S. Verma, J. Choudhary, K.P. Singh, P. Chandra, S.P. Singh, Uricase grafted nanoconducting matrix based electrochemical biosensor for ultrafast uric acid detection in human serum samples, *Inter. J. Biol. Macromol.* 130 (2019) 333–341.
- [40] M. Roostaeae, I. Sheikhshoaie, Fabrication of a sensitive sensor for determination of xanthine in the presence of uric acid and ascorbic acid by modifying a carbon paste sensor with Fe₃O₄@Au core-shell and an ionic liquid, *J. Food Meas. Charact.* 16 (2022) 731–739.
- [41] K. Rajalakshmi, S. Abraham John, Selective determination of mefenamic acid in the presence of 1000-fold excess paracetamol and caffeine using a multiwalled carbon nanotube-polymer composite electrode, *Anal. Meth.* 7 (2015) 3506–3511.
- [42] R. Ojani, A. Alinezhad, Z. Abedi, A highly sensitive electrochemical sensor for simultaneous detection of uric acid, xanthine and hypoxanthine based on poly(l-methionine) modified glassy carbon electrode, *Sens. Actuat. B: Chem.* 188 (2013) 621–630.
- [43] L. Lin, C. Song, L. Xie, L. Yu, L. Wu, M. Zhang, S. Yang, H. Gao, X. Li, Electrochemical determination of xanthine and hypoxanthine in rat striatum with an acetylene black-dihexadecyl hydrogen phosphate composite film modified electrode by HPLC coupled with in vivo microdialysis, *Microchim. Acta* 170 (2010) 47–52.
- [44] F. Zhang, Z. Wang, Y. Zhang, Z. Zheng, C. Wang, Y. Du, W. Ye, Simultaneous electrochemical determination of uric acid, xanthine and hypoxanthine based on poly(l-arginine)/graphene composite film modified electrode, *Talanta* 93 (2012) 320–325.
- [45] K. Rajalakshmi, S. Abraham John, Highly sensitive determination of nitrite using FMWCNTs-conducting polymer composite modified electrode, *Sens. Actuat. B* 215 (2015) 119–124.
- [46] R.N. Goyal, V.K. Gupta, S. Chatterjee, Simultaneous determination of adenosine and inosine using single-wall carbon nanotubes modified pyrolytic graphite electrode, *Talanta* 76 (2008) 662–668.
- [47] K. Rajalakshmi, S. Abraham John, Chemical attachment of functionalized multiwalled carbon nanotubes on glassy carbon electrode for electrocatalytic application, *Electrochim. Acta* 165 (2015) 268–276.
- [48] R. Thangaraj, A.S. Kumar, Graphitized mesoporous carbon modified glassy carbon electrode for selective sensing of xanthine, hypoxanthine and uric acid, *Anal. Meth.* 4 (2012) 2162–2171.

| | |
|--|----------------|
| 委托人单位 | 镇江市第一人民医院 |
| 委 托 人 | 刘晓健 |
| 检 索 要 求 | SCIE 论文收录及期刊分区 |
| 检 索 时 段 | 2024-2024 |
| 检 索 结 果 | |
| 数 据 库 | 论文收录(篇)及引用情况 |
| SCIE, 中国科学院文献 情报中心期刊分区表 升级版 | SCIE 收录论文 1 篇. |
| <p>SCIE 论文题录:</p> <p>1. 标题: Simultaneous and selective determination of purine metabolites in human urine samples using nanocomposite modified glassy carbon electrode</p> <p>作者: Liu, XJ (Liu, Xiaojian); Dai, JD (Dai, Jindong); Shen, J (Shen, Jian); Zhu, DW (Zhu, Dongwei); Rajalakshmi, K (Rajalakshmi, Kanagaraj); Muthusamy, S (Muthusamy, Selvaraj); Kanagaraj, T (Kanagaraj, Thangamani); Kannan, P (Kannan, Palanisamy)</p> <p>来源出版物: JOURNAL OF MOLECULAR LIQUIDS 卷: 411 文献号: 125845 DOI: 10.1016/j.molliq.2024.125845 Published Date: 2024 OCT 1</p> <p>Web of Science 核心合集中的 "被引频次": 0</p> <p>被引频次合计: 0</p> <p>入藏号: WOS:001317067000001</p> <p>文献类型: Article</p> <p>地址: [Liu, Xiaojian; Dai, Jindong; Shen, Jian; Zhu, Dongwei; Rajalakshmi, Kanagaraj; Muthusamy, Selvaraj; Kanagaraj, Thangamani] Jiangsu Univ, Affiliated Peoples Hosp, Dept Gynecol, Zhenjiang 212013, Peoples R China.</p> <p>[Liu, Xiaojian; Dai, Jindong; Shen, Jian; Zhu, Dongwei; Rajalakshmi, Kanagaraj; Muthusamy, Selvaraj; Kanagaraj, Thangamani] Jiangsu Univ, Sch Med, Dept Immunol, Jiangsu Key Lab Lab Med, Zhenjiang 212013, Peoples R China.</p> <p>[Liu, Xiaojian; Dai, Jindong; Shen, Jian; Zhu, Dongwei; Rajalakshmi, Kanagaraj; Muthusamy, Selvaraj; Kanagaraj, Thangamani] Jiangsu Univ, Sch Chem & Chem Engn, Zhenjiang 212013, Peoples R China.</p> <p>[Kannan, Palanisamy] Jiaxing Univ, Coll Biol Chem Sci & Engn, Jiaxing 314001, Zhejiang, Peoples R China.</p> | |

通讯作者地址: Rajalakshmi, K; Muthusamy, S (通讯作者), Jiangsu Univ, Affiliated Peoples Hosp, Dept Gynecol, Zhenjiang 212013, Peoples R China.

Rajalakshmi, K; Muthusamy, S (通讯作者), Jiangsu Univ, Sch Med, Dept Immunol, Jiangsu Key Lab Lab Med, Zhenjiang 212013, Peoples R China.

Rajalakshmi, K; Muthusamy, S (通讯作者), Jiangsu Univ, Sch Chem & Chem Engr, Zhenjiang 212013, Peoples R China.

Kannan, P (通讯作者), Jiaying Univ, Coll Biol Chem Sci & Engr, Jiaying 314001, Zhejiang, Peoples R China.

电子邮件地址: rajichen89@ujs.edu.cn; rajselsva311@ujs.edu.cn; ktpkannan@zjxu.edu.cn

ISSN: 0167-7322

eISSN: 1873-3166

中国科学院文献情报中心期刊分区表升级版

首页 博客 反馈 退出

2023年 -

JOURNAL OF MOLECULAR LIQUIDS

| | | | |
|----------------|--|----|-------|
| 刊名 | JOURNAL OF MOLECULAR LIQUIDS | | |
| 年份 | 2023 | | |
| ISSN | 0167-7322 | | |
| Review | 否 | | |
| Open Access | 否 | | |
| Web of Science | SCIE | | |
| | 学科 | 分区 | Top期刊 |
| 大类 | 化学 | 2 | 是 |
| 小类 | PHYSICS, ATOMIC, MOLECULAR & CHEMICAL 物理: 原子、分子和化学物理 | 1 | |
| | CHEMISTRY, PHYSICAL 物理化学 | 2 | - |

备注:结果见附件.

委托人(签字)

刘晓明

检索人(签字): 刘晓男

审核人(签字)

江苏大学图书馆

(情报检索业务专用章)

2024年10月08日

第 1 条, 共 1 条

标题: Simultaneous and selective determination of purine metabolites in human urine samples using nanocomposite modified glassy carbon electrode

作者: Liu, XJ (Liu, Xiaojian); Dai, JD (Dai, Jindong); Shen, J (Shen, Jian); Zhu, DW (Zhu, Dongwei); Rajalakshmi, K (Rajalakshmi, Kanagaraj); Muthusamy, S (Muthusamy, Selvaraj); Kanagaraj, T (Kanagaraj, Thangamani); Kannan, P (Kannan, Palanisamy)

来源出版物: JOURNAL OF MOLECULAR LIQUIDS 卷: 411 文献号: 125845 DOI: 10.1016/j.molliq.2024.125845 Published Date: 2024 OCT 1

Web of Science 核心合集中的 "被引频次": 0

被引频次合计: 0

使用次数 (最近 180 天): 0

使用次数 (2013 年至今): 0

引用的参考文献数: 48

入藏号: WOS:001317067000001

语言: English

文献类型: Article

作者关键词: Carbon nanotube; Polymer; Composite; Simultaneous determination; Lowest limit of detection

KeyWords Plus: HYPOXANTHINE; XANTHINE; INOSINE; ACID; NANOTUBES; ADENOSINE; SENSOR

地址: [Liu, Xiaojian; Dai, Jindong; Shen, Jian; Zhu, Dongwei; Rajalakshmi, Kanagaraj; Muthusamy, Selvaraj; Kanagaraj, Thangamani] Jiangsu Univ, Affiliated Peoples Hosp, Dept Gynecol, Zhenjiang 212013, Peoples R China.

[Liu, Xiaojian; Dai, Jindong; Shen, Jian; Zhu, Dongwei; Rajalakshmi, Kanagaraj; Muthusamy, Selvaraj; Kanagaraj, Thangamani] Jiangsu Univ, Sch Med, Dept Immunol, Jiangsu Key Lab Lab Med, Zhenjiang 212013, Peoples R China.

[Liu, Xiaojian; Dai, Jindong; Shen, Jian; Zhu, Dongwei; Rajalakshmi, Kanagaraj; Muthusamy, Selvaraj; Kanagaraj, Thangamani] Jiangsu Univ, Sch Chem & Chem Engr, Zhenjiang 212013, Peoples R China.

[Kannan, Palanisamy] Jiaxing Univ, Coll Biol Chem Sci & Engr, Jiaxing 314001, Zhejiang, Peoples R China.

通讯作者地址: Rajalakshmi, K; Muthusamy, S (通讯作者), Jiangsu Univ, Affiliated Peoples Hosp, Dept Gynecol, Zhenjiang 212013, Peoples R China.

Rajalakshmi, K; Muthusamy, S (通讯作者), Jiangsu Univ, Sch Med, Dept Immunol, Jiangsu Key Lab Lab Med, Zhenjiang 212013, Peoples R China.

Rajalakshmi, K; Muthusamy, S (通讯作者), Jiangsu Univ, Sch Chem & Chem Engr, Zhenjiang 212013, Peoples R China.

Kannan, P (通讯作者), Jiaxing Univ, Coll Biol Chem Sci & Engr, Jiaxing 314001, Zhejiang, Peoples R China.

电子邮件地址: rajichen89@ujs.edu.cn; rajselsa311@ujs.edu.cn; ktpkannan@zjxu.edu.cn

Affiliations: Jiangsu University; Jiangsu University; Jiangsu University; Jiaxing University

作者识别号:

| 作者 | Web of Science ResearcherID | ORCID 号 |
|--------------------|-----------------------------|---------|
| Kannan, Palanisamy | E-7198-2011 | |

出版商: ELSEVIER

出版商地址: RADARWEG 29, 1043 NX AMSTERDAM, NETHERLANDS

Web of Science Index: Science Citation Index Expanded (SCI-EXPANDED)

Web of Science 类别: Chemistry, Physical; Physics, Atomic, Molecular & Chemical

研究方向: Chemistry; Physics

IDS 号: G5M1X

ISSN: 0167-7322

eISSN: 1873-3166

29 字符的来源出版物名称缩写: J MOL LIQ

ISO 来源出版物缩写: J. Mol. Liq.

来源出版物页码计数: 9

基金资助致谢:

| 基金资助机构 | 授权号 |
|--|-----------|
| National Natural Science Foundation of China | 82202001 |
| Project of Jiangsu Provincial Administration of Traditional Chinese Medicine | MS2023144 |

| | |
|--|-------------|
| Project of Zhenjiang Science and Technology Bureau | SH2023066 |
| National Natural Science Foundation of China | 22150410327 |

D.Z thanks to National Natural Science Foundation of China (Grant Nos. 82202001) , X. L thanks for the Project of Jiangsu Provincial Administration of Traditional Chinese Medicine (MS2023144) and Project of Zhenjiang Science and Technology Bureau (SH2023066) and S. M Thanks to the National Natural Science Foundation of China (No. 22150410327) .

输出日期: 2024-10-08

End of File